

This is the **accepted version** of the journal article:

Karami-Horestani, Amirhossein; Paredes, Ferran; Saura, Karl Adolphs; [et al.].
«Capacitive Sensor for Micrometer-Scale Proximity Detection with Microwaves».
IEEE Sensors Journal, (2025). DOI 10.1109/JSEN.2025.3527691

This version is available at <https://ddd.uab.cat/record/306116>

under the terms of the  ^{IN}
COPYRIGHT license

Capacitive Sensor for Micrometer-Scale Proximity Detection with Microwaves

Amirhossein Karami-Horestani, *Graduate Student Member, IEEE*, Ferran Paredes, *Senior Member, IEEE*, Karl Adolphs, Amir Ebrahimi, *Member, IEEE*, and Ferran Martín, *Fellow, IEEE*

Abstract—This paper presents a highly sensitive proximity sensor with micrometer-scale resolution. The working principle is the change in the capacitance of a movable step-impedance resonator (SIR), in relative (vertical) motion with respect to the static part, a pair of matched lines terminated with a patch capacitance and sharing the same axis. If the patches of the lines are aligned with the SIR patches, the resulting structure is a two-port device loaded with a series connected resonator with variable capacitance (caused by the SIR vertical motion). The output signal of the reported proximity sensor is the phase of the transmission coefficient at the operating frequency. Such frequency can (canonically) be the resonance frequency of the SIR when the substrate where such element is etched is in contact with the static part, but the device can be tuned to different operating frequencies, opening the possibility to further enhance the sensitivity. Thus, this transmission-mode phase-variation sensor is a single-frequency device (this simplifies the electronics required for sensor feeding and processing in situations where a vector network analyzer cannot be used). An exhaustive sensitivity analysis for sensor operation at the resonance frequency of the SIR is carried out in the paper. According to such an analysis, it is concluded that for sensitivity (and resolution) optimization, the SIR must be designed with a long narrow strip and small metal patches. Nevertheless, from a simulation-based analysis, it is shown that the sensitivity can be dramatically boosted up by device operation at the frequency where the phase of the transmission coefficient is $\pm 180^\circ$, provided the static part substrate is adequately chosen. Three prototype proximity sensors are presented and experimentally validated to demonstrate all these aspects. The achieved maximum sensitivity, resolution, and dynamic range in one of such prototypes are $4485^\circ/\text{mm}$, $5\text{ }\mu\text{m}$, and 0.1 mm , respectively.

Index Terms—Capacitive sensor, displacement sensor, microstrip technology, microwave sensor, phase-variation sensor, proximity sensor, step-impedance resonator (SIR), transmission-mode sensor.

I. INTRODUCTION

PROXIMITY sensors are devices that can detect the presence or approach of nearby objects [1]. Certain proximity sensors use the eddy currents that are generated in metallic sensing objects by electromagnetic induction [2], [3]. Detecting changes in an electrical capacitance caused by an approaching sensing object is another working principle used in proximity sensors [4]–[7]. There are also systems that use magnetic induction to detect proximity [8], [9]. Additional technologies for proximity sensing include ultrasounds [10]–[12], laser systems [13]–[15] and infrared systems [16], [17].

In this paper, we propose a contactless capacitive-type proximity sensor able to detect the presence and determine the relative position of the moving object with micrometer-scale resolution, provided it is located at distances below 1 mm from the sensing (static) element. The position of the moving object, a thin dielectric slab with a step-impedance resonator (SIR) etched on one of its faces, is determined by means of microwaves. Specifically, the sensor (static part) is a planar two-port structure fed by a harmonic (single frequency)

microwave signal, and the output variable is the phase of the transmission coefficient at that frequency. Such phase varies when the movable SIR displaces vertically, due to the change in the capacitance of the series-connected resonator formed by the SIR and the static element.

Planar microwave technology has been profusely used in motion sensors, including low range displacement sensors [18]–[31] and moderate/high dynamic range displacement and velocity sensors [32]–[49]. Among the latter type of sensors, electromagnetic encoders (either linear or angular) [34]–[49] have been demonstrated to be good competitors to the well-known optical encoders [50]–[52], magnetic encoders [53], [54], and Hall-effect sensors [55]–[60]. Namely, as compared to their optical counterparts, electromagnetic (or microwave) encoders are robust against pollution and dirtiness, encountered in many industrial systems. On the other hand, electromagnetic encoders do not use magnets or inductive coils, thereby representing a low-cost solution as compared to magnetic encoders and Hall-effect sensors. Other advantages of planar microwave sensors include small size and low profile, easy

This work was supported by MCIN/AEI 10.13039/501100011033, Spain, through the project PID2022-139181OB-I00 (ERDF European Union) and by the AGAUR Research Agency, Catalonia Government, through the project 2021SGR-00192. A. Karami-Horestani acknowledges MCIN/AEI /10.13039/501100011033 and ESF for Grant PRE2020-093239. The work of A. Ebrahimi was supported by a CASS Foundation Medicine/Science Grant under Project 10386.

A. Karami-Horestani, F. Paredes, K. Adolphs, and F. Martín are with GEMMA/CIMITEC, Departament d'Enginyeria Electrònica, Universitat Autònoma de Barcelona, 08193 Bellaterra, Spain. (e-mail: Amirhossein.Karami@uab.cat).

A. Ebrahimi is with the School of Engineering, Royal Melbourne Institute of Technology (RMIT) University, Melbourne, VIC 3001, Australia.

implementation in a wide variety of substrates (rigid, flexible, polymeric, organic, textiles, etc.) by means of subtractive (e.g., photoetching or milling) or additive (e.g., printing) processes, possibility of integration of the sensor electronics (necessary for feeding and post-processing in a real scenario) in the sensor substrate, and their inherent wireless connectivity (as far as microwave radiation is involved) [61]. It is also remarkable the use of dielectric resonators for motion sensing [62]–[65].

It has been recently demonstrated that planar microwave sensors that utilize the phase of the reflection coefficient as the output variable exhibit unprecedented sensitivities, provided they are adequately designed [29], [30], [66]–[74]. Most of these devices are permittivity sensors [66]–[74]. However, some of them have been used as proximity sensors [71], [74], by virtue of the changes in the effective permittivity that results by separating a dielectric slab from the sensitive element (typically a planar resonator, either distributed or semi-lumped). The reported sensitivities in such proximity sensors are very competitive. However, in a recent paper [75], sensitivities of thousands of degrees per mm have been achieved in a reflective-mode phase-variation proximity sensor by using a variable capacitance (specifically, the capacitance of a SIR resonator etched in a movable substrate in relative motion to the static part, an open-ended coplanar waveguide –CPW).

In this paper, we report a single-frequency phase-variation proximity sensor also based on a movable SIR resonator, but operating in transmission, and with the static part implemented in microstrip technology. The paper is organized as follows. Section II presents the proposed proximity sensor, the working principle (in detail), and the circuit model. The model is validated in such section from parameter extraction. Section III is devoted to the sensitivity analysis for sensor operation at the SIR resonance frequency, where an analytical expression providing an estimation of the sensitivity in the limit of small vertical displacements of the movable SIR is obtained. The validation of the previous analysis and sensor functionality are reported in Section IV from full wave electromagnetic simulation and experiments. It is also shown in this section that by considering alternative frequencies of operation, the sensitivity can be further boosted up. In section V, a comparative analysis with other microwave proximity sensors is carried out. Finally, section VI concludes the work.

II. THE PROPOSED PROXIMITY SENSOR, WORKING PRINCIPLE, AND EQUIVALENT CIRCUIT MODEL

The proposed proximity sensor consists of two parts. The static part is a two-port structure that can be viewed as a pair of transmission lines terminated with a capacitive patch, oppositely oriented and sharing the same axis (see Fig. 1). The movable part is a low-loss thin dielectric slab with an SIR etched on it (see also Fig. 1). The size of the SIR patches is slightly smaller than the size of the patches terminating the lines. Thus, when the axis of the SIR is aligned with the axis of the lines, and the SIR patches are on top the line patches, a series resonator, generated by the capacitance between the patches and by the narrow (inductive) strip of the SIR, appears.

The capacitance of such resonator depends on the vertical distance between the SIR and line patches. Thus, it is expected that the transmission coefficient of the resulting two-port structure depends on the proximity between the dielectric slab of the SIR and the substrate of the static part. In particular, a variation in the resonance frequency, close to the frequency of maximum transmission is expected. Such resonance frequency can be used as output variable for sensing, as in many reported frequency-variation sensors (see [61], chapter 2). However, in this paper we opt, as a first option, for considering as output variable the phase of the transmission coefficient at the resonance frequency when the SIR substrate rests on top of the static part (reference – REF– position). This is the most canonical frequency of operation. Nevertheless, we will discuss later the possibility of considering different frequencies of operation (with an eye towards sensitivity optimization).

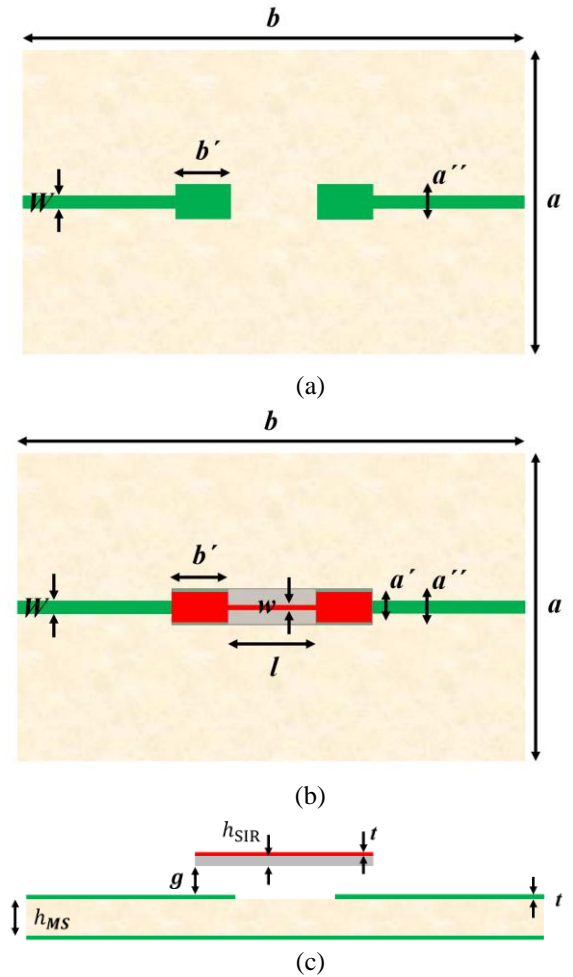


Fig. 1. Top view of the static part (a), top view of the movable element (SIR) lying on top of the static part (b), and cross-sectional view of the proposed sensor (c) for an arbitrary vertical distance, g , between the SIR substrate and the static part. For validation of the model, the considered dimensions (in mm) for sensor A (first prototype) are: $a = 50$, $b = 60$, $W = 1.19$, $b' = 5$, $l = 10$, $w = 0.4$, $a' = 2.6$, $a'' = 3.1$, $h_{MS} = 0.508$, $h_{SIR} = 0.81$, and $t = 0.035$. All these dimensions are the same for the other (two) designed and fabricated sensors, except h_{MS} and h_{SIR} , and hence W , which needs to be modified to implement 50- Ω microstrip access lines in all cases. Note that a' is the width of the SIR substrate, identical to the width of the microstrip patch termination.

Note that a window in the ground plane of the static part has been etched. Such window has a length identical to the length of the narrow strip of the SIR (or distance between patches), and it has the mere purpose of minimizing the variation of the SIR inductance with the vertical distance. There is not an *a priori* reason that justifies keeping a constant inductance, but the sensitivity analysis to be carried out in Section III is simplified by considering that the unique variable element with the vertical distance is the SIR capacitance.

Let us clarify that the proposed proximity sensor is conceived to measure vertical displacement with proper alignment between the static part and the movable part (the SIR), i.e., as shown in Fig. 1(b). Namely, during vertical motion of the SIR, the axis of the SIR and the axis of the access lines are perfectly aligned.

The circuit model of the proposed proximity sensor is depicted in Fig. 2. In this model, L is the SIR inductance, related to the length and width of the narrow strip, and considered constant, as justified in the previous paragraph, and C_p is the capacitance of the patches terminating the lines of the static element to ground, also considered constant (i.e., not dependent on the vertical distance, g , between the SIR substrate and the static part). Finally, C is the overall capacitance of the SIR, composed of the series connection of the capacitances between the SIR patches and the line patches (such capacitances are designated as C_s , and, therefore, $C = C_s/2$). The capacitance C depends on the vertical distance g , and it can be expressed as $C = C_{\text{REF}} + \Delta C$, where C_{REF} is the SIR capacitance when the SIR substrate rests on top of the static part (REF position, or $g = 0$ mm) and ΔC is the variation of the capacitance when an arbitrary distance is considered (note that ΔC is negative).

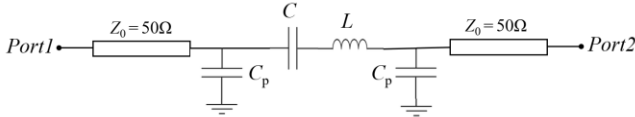


Fig. 2. Equivalent circuit model of the proposed sensor. Losses are neglected in the model, as far as low loss microwave substrates for the static element and SIR are considered.

To validate the proposed circuit model of the sensor, a parameter extraction procedure is needed. Since the model depends on three reactive elements, L , C and C_p , three conditions are required. One of such conditions is the angular resonance frequency of the SIR, given by:

$$\omega_0 = \frac{1}{\sqrt{LC}} \quad (1)$$

Such frequency can be identified from the intersection of the reflection coefficient with the unit conductance circle in the Smith chart (the presence of the access lines is neglected). Reading the susceptance value at that frequency (second condition), the capacitance C_p is directly inferred. Finally, the third condition can be, e.g., the slope of the phase of the transmission coefficient at resonance. Therefore, it is necessary to obtain the phase of the transmission coefficient. The transmission coefficient is given by [76]

$$S_{21} = \frac{2}{A + \frac{B}{Z_0} + Z_0 C + D} \quad (2)$$

where A , B , C , and D are the element values of the transmission ABCD matrix, A , and Z_0 is the reference impedance of the ports ($Z_0 = 50 \Omega$ in this work). Such matrix is the product of the transmission matrices of the three cascaded two-port networks, i.e., the two shunt-connected capacitances C_p , and the series LC resonator in between [76]:

$$\mathbf{A} = \begin{pmatrix} A & B \\ C & D \end{pmatrix} = \begin{pmatrix} 1 & 0 \\ Y & 1 \end{pmatrix} \begin{pmatrix} 1 & Z \\ 0 & 1 \end{pmatrix} \begin{pmatrix} 1 & 0 \\ Y & 1 \end{pmatrix} = \begin{pmatrix} 1 + YZ & Z \\ 2Y + ZY^2 & 1 + YZ \end{pmatrix} \quad (3)$$

with

$$Y = j\omega C_p \quad (4a)$$

$$Z = j\omega L \left(1 - \frac{\omega_0^2}{\omega^2} \right) \quad (4b)$$

ω being the angular frequency.

Introducing (4) in (3), and the matrix elements in (2), the transmission coefficient is found to be:

$$S_{21} = \frac{2}{2 - 2LC_p\omega^2 \left(1 - \frac{\omega_0^2}{\omega^2} \right) + j \left\{ 2Z_0\omega C_p + \left(1 - \frac{\omega_0^2}{\omega^2} \right) \left(\frac{\omega L}{Z_0} - Z_0\omega^3 C_p^2 L \right) \right\}} \quad (5)$$

The phase of the transmission coefficient, ϕ_T , is thus:

$$\phi_T = -\arctan \left\{ \frac{2Z_0\omega C_p + \left(1 - \frac{\omega_0^2}{\omega^2} \right) \left(\frac{\omega L}{Z_0} - Z_0\omega^3 C_p^2 L \right)}{2 - 2LC_p\omega^2 \left(1 - \frac{\omega_0^2}{\omega^2} \right)} \right\} \quad (6)$$

and the phase slope is:

$$\frac{d\phi_T}{d\omega} = -\frac{1}{1 + \left(\frac{N_a}{D_a} \right)^2} \cdot \frac{D_a N_a' - N_a D_a'}{D_a^2} \quad (7)$$

where N_a and D_a are the numerator and the denominator, respectively, of the argument of the arctan in (6), and N_a' and D_a' are their derivatives with the angular frequency, given by:

$$N_a' = \frac{L}{Z_0} \left(1 + \frac{\omega_0^2}{\omega^2} \right) + 2Z_0 C_p - Z_0 C_p^2 L (3\omega^2 - \omega_0^2) \quad (8a)$$

$$D_a' = -4LC_p\omega \quad (8b)$$

Finally, evaluation of the phase slope at resonance gives:

$$\left. \frac{d\phi_T}{d\omega} \right|_{\omega_0} = -\frac{\frac{L}{Z_0} + Z_0 C_p + Z_0 C_p^2 L \omega_0^2}{1 + Z_0^2 \omega_0^2 C_p^2} \quad (9)$$

Note that expression (9) does not depend on C . Consequently, once C_p is known [see the paragraph above expression (2)], L can be isolated from (9), provided the phase slope at resonance is inferred from electromagnetic simulation. Finally, C is obtained from (1).

The previous parameter extraction method was applied to the structure of Fig 1, with dimensions indicated in the caption. The considered substrate for the static part is the *Rogers 4003C*

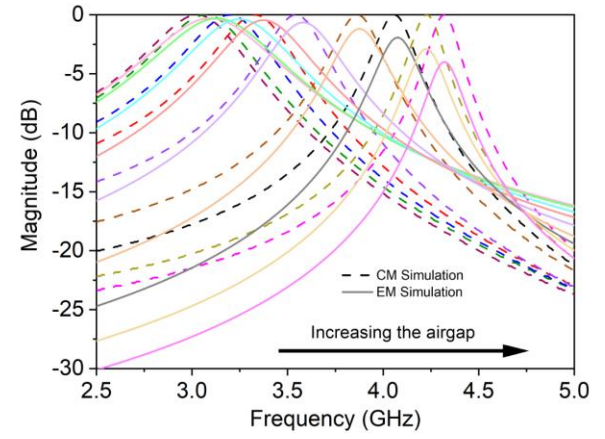
with dielectric constant $\epsilon_r = 3.55$, thickness $h_{MS} = 0.508$ mm, and loss tangent $\tan\delta = 0.0022$. For the SIR, the considered substrate is the *Rogers 4003C* with dielectric constant $\epsilon_{SIR} = 3.55$, thickness $h_{SIR} = 0.81$ mm, and loss tangent $\tan\delta_{SIR} = 0.0022$. Nevertheless, losses are neglected in the simulation, in coherence with the circuit model. Such lossless approximation is reasonable as far as the substrates of the SIR and static element are made of low-loss materials. In Fig. 3 the magnitude and the phase response of the transmission coefficient, as well as the reflection coefficient in the Smith chart, are depicted. Indeed, Fig. 3 depicts the responses of the sensor for various vertical distances, g , up to 1 mm. For all the considered values of g , we have extracted the reactive parameters (see Table I). According to the table, C_p does not significantly vary with g , as expected. The inductance L varies smoothly (less than 23%) for separations below (roughly) 0.2 mm, and then the change is more significant (nevertheless, the sensitivity analysis in Section III is focused on obtaining the sensitivity in the limit of small separations, where L is roughly constant, in coherence with the hypotheses of that analysis). Concerning the capacitance C , it experiences a significant variation, especially for small values of g . The agreement between the electromagnetic simulations and the circuit simulations with extracted parameters is reasonably good for all the values of g . Discrepancies in the magnitude response of Fig. 3(a) are in part attributed to the fact that losses in the circuit model have been ignored. The electromagnetic simulations do not include ohmic and dielectric losses, but certain losses due to radiation are unavoidable in practice (this has been corroborated from electromagnetic simulations, not shown). The results of Fig. 3 validate the model and the parameter extraction procedure.

TABLE I

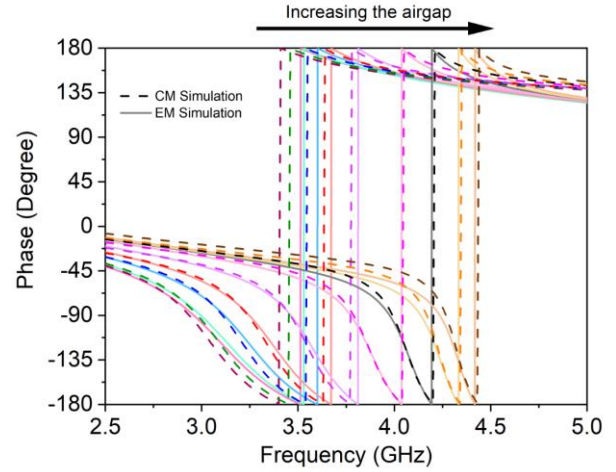
EXTRACTED REACTIVE PARAMETERS OF THE CIRCUIT MODEL

g (mm)	C_p (pF)	L (nH)	C (pF)
0.00	1.572	11.20	0.315
0.01	1.550	11.14	0.307
0.05	1.528	11.88	0.258
0.10	1.527	12.26	0.226
0.20	1.527	13.76	0.171
0.40	1.480	15.31	0.125
0.60	1.450	17.66	0.096
0.80	1.440	19.95	0.077
1.00	1.350	22.90	0.064

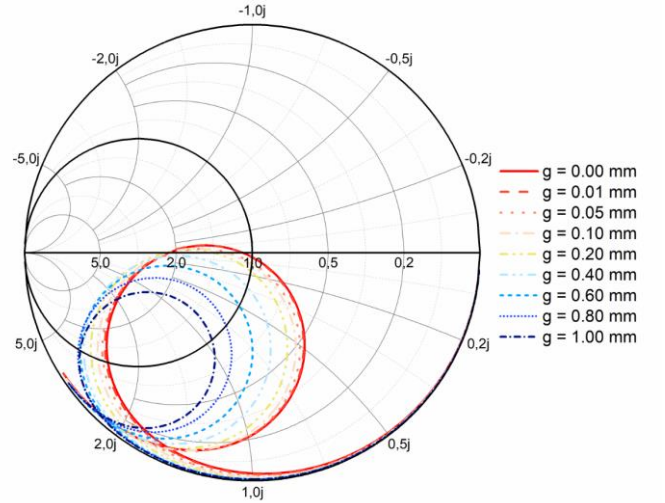
Let us clarify that in the responses shown in Fig. 3, the effects of the access lines have been ignored (by de-embedding). Naturally, in the fabricated sensor, to be discussed later, not only access lines but also connectors are needed, but the sensor operates at a single frequency, and hence such lines and connectors add a constant phase shift that can be ignored.



(a)



(b)



(c)

Fig. 3. Magnitude (a) and phase (b) of the transmission coefficient as inferred from circuit model (CM) simulation with extracted parameters and electromagnetic (EM) simulation, and representation of the reflection coefficient in the Smith chart as inferred from EM simulation (c), corresponding to different values of g (indicated). Dimensions are indicated in the caption of Fig. 1 and correspond to the reference sensor, designated as sensor A. The electromagnetic simulations have been carried out by means of the Ansys *HFSS* commercial software.

III. SENSITIVITY ANALYSIS

The sensitivity is defined as the variation of the phase of the transmission coefficient at the operating frequency with the vertical distance, g . Since g has only an appreciable effect on C , at least in the limit of small separations, the sensitivity can be approximated as

$$\frac{d\phi_T}{dg} = \frac{d\phi_T}{dC} \cdot \frac{dC}{dg} = \frac{d\phi_T}{d\Delta C} \cdot \frac{d\Delta C}{dg} \quad (10)$$

provided $C = C_{\text{REF}} + \Delta C$ and C_{REF} , the capacitance in the REF position ($g = 0$ mm), is a constant. In order to obtain the first derivative in the right-hand side member of (10), let us evaluate the phase of the transmission coefficient for an arbitrary distance g , or arbitrary capacitance C , at the (canonical) operating angular frequency, i.e., the resonance frequency of the SIR, given by (1), for the REF position, i.e.,

$$\omega_{0,\text{REF}} = \frac{1}{\sqrt{LC_{\text{REF}}}} \quad (11)$$

For that purpose, we have to rewrite expression (6) with ω replaced with $\omega_{0,\text{REF}}$, and ω_0 expressed as:

$$\omega_0 = \frac{1}{\sqrt{LC}} = \frac{1}{\sqrt{L(C_{\text{REF}} + \Delta C)}} = \frac{\omega_{0,\text{REF}}}{\sqrt{1 + \frac{\Delta C}{C_{\text{REF}}}}} \quad (12)$$

The following result is obtained:

$$= -\arctan \left\{ \frac{\phi_T(\omega_{0,\text{REF}}) = \left(\frac{2Z_0\omega_{0,\text{REF}}C_p + \left(\frac{\Delta C}{C_{\text{REF}} + \Delta C} \right) \left(\frac{\omega_{0,\text{REF}}L}{Z_0} - Z_0\omega_{0,\text{REF}}^3C_p^2L \right) \right)}{2 - 2LC_p\omega_{0,\text{REF}}^2 \left(\frac{\Delta C}{C_{\text{REF}} + \Delta C} \right)} \right\} \quad (13)$$

The derivative of (13) with ΔC is:

$$\frac{d\phi_T(\omega_{0,\text{REF}})}{d\Delta C} = -\frac{1}{1 + \left(\frac{N_A}{D_A} \right)^2} \cdot \frac{D_A N_A' - N_A D_A'}{D_A^2} \quad (14)$$

where N_A and D_A are the numerator and the denominator, respectively, of the argument of the arctan in (13), and N_A' and D_A' are their derivatives with ΔC , given by:

$$N_A' = \left(\frac{\omega_{0,\text{REF}}L}{Z_0} - Z_0\omega_{0,\text{REF}}^3C_p^2L \right) \frac{C_{\text{REF}}}{(C_{\text{REF}} + \Delta C)^2} \quad (15a)$$

$$D_A' = -2LC_p\omega_{0,\text{REF}}^2 \frac{C_{\text{REF}}}{(C_{\text{REF}} + \Delta C)^2} \quad (15b)$$

Since the considered proximity sensor is intended to detect very small vertical displacements, the interest is the sensitivity in the limit when $g = 0$ mm, or $\Delta C = 0$ pF. In such limit, (14) gives (after some algebra):

$$\left. \frac{d\phi_T(\omega_{0,\text{REF}})}{d\Delta C} \right|_{\Delta C=0} = -\frac{\omega_{0,\text{REF}}L}{2Z_0C_{\text{REF}}} = -\frac{1}{2Z_0C_{\text{REF}}\omega_{0,\text{REF}}} \quad (16)$$

Interestingly, (16) does not depend on C_p . Hence, an identical result is obtained in a hypothetical structure where the patch capacitance to ground can be neglected, i.e., merely described by a series connected LC resonator.

The last derivative in the right-hand side member of (10) can be analytically calculated by considering valid the parallel-plate

capacitor formula. This approximation is reasonable as far as the vertical distance between the SIR patches and the terminating patches of the lines ($g + h_{\text{SIR}}$) is much smaller than the side length of the SIR patches. Nevertheless, by considering such an approximation, an estimation, rather than an accurate prediction of the sensitivity, is obtained, as it will be later discussed. Let A_p be the area of one of the SIR patches. The capacitance C can be expressed as [76]:

$$C = \frac{C_s}{2} = \frac{A_p\epsilon_0}{2} \cdot \frac{\epsilon_{r,\text{SIR}} \cdot \frac{1}{h_{\text{SIR}}}}{\frac{\epsilon_{r,\text{SIR}}}{h_{\text{SIR}}} + \frac{1}{g}} = \frac{A_p\epsilon_0}{2} \cdot \frac{\epsilon_{r,\text{SIR}}}{g\epsilon_{r,\text{SIR}} + h_{\text{SIR}}} \quad (17)$$

where ϵ_0 is the permittivity of vacuum, and $\epsilon_{r,\text{SIR}}$ and h_{SIR} are the dielectric constant and thickness, respectively, of the SIR substrate. Deriving (17) with g , we obtain:

$$\frac{dC}{dg} = \frac{d\Delta C}{dg} = -\frac{A_p\epsilon_0}{2} \cdot \frac{\epsilon_{r,\text{SIR}}^2}{(g\epsilon_{r,\text{SIR}} + h_{\text{SIR}})^2} = -\frac{\epsilon_{r,\text{SIR}}C}{g\epsilon_{r,\text{SIR}} + h_{\text{SIR}}} \quad (18)$$

and the previous result in the limit of small separations ($g = 0$ mm) simplifies to

$$\left. \frac{d\Delta C}{dg} \right|_{\Delta C=0, g=0} = -\frac{\epsilon_{r,\text{SIR}}C_{\text{REF}}}{h_{\text{SIR}}} = -\frac{2C_{\text{REF}}^2}{A_p\epsilon_0} \quad (19)$$

Introducing (16) and (19) in (10), the sensitivity in the limit of small separations between the SIR substrate and the static part ($g = 0$ mm) is found to be:

$$\left. \frac{d\phi_T(\omega_{0,\text{REF}})}{dg} \right|_{\Delta C=0, g=0} = \frac{1}{A_p\epsilon_0 Z_0 \omega_{0,\text{REF}}} \quad (20)$$

According to (20), to boost the sensitivity, it is necessary to deal with small SIR patches (A_p small). Decreasing the frequency of operation, $\omega_{0,\text{REF}}$, also benefits the sensitivity. Since the reduction of the area of the patches decreases the SIR capacitance, it is necessary to consider narrow and long SIR strips in order to achieve a relatively high SIR inductance, L , able to drive the operating frequency to relatively low values. Thus, for sensitivity optimization, SIRs exhibiting a narrow and elongated central strip and small patches are convenient. Note that the previous sensitivity analysis explicitly considers that the sensing element is an SIR resonator in expression (17), where the parallel plate capacitor formula has been used. Thus, this analysis would be of application to other sensing resonators where the capacitance can be approximated by such a formula.

It is interesting to mention that expression (20) differs from the corresponding expression of the CPW reflective-mode SIR-based proximity sensor reported in [75] (operating at the resonance frequency of the SIR) by a factor of 4. Even though the sensor proposed in this paper operates in transmission and is implemented in microstrip technology, the dependence of the sensitivity on A_p , ϵ_0 , Z_0 , and $\omega_{0,\text{REF}}$ is identical (i.e., inversely proportional). Although the sensitivity in the limit of small vertical displacements is 4 times larger in the proximity sensor of [75], the (4 times) smaller sensitivity of the proposed transmission-mode phase-variation sensor can be compensated by reducing A , $\omega_{0,\text{REF}}$, or both parameters simultaneously. In

other words, the achievable sensor performance, measured in terms of the maximum sensitivity, is comparable in both sensors. Moreover, the frequency of operation of the sensor can be set to different values, providing (in certain cases) significantly improved sensitivities, as will be discussed later. Particularly, we can consider operation at the frequency where the phase of the reflection coefficient is $\phi_r = -90^\circ$, when the movable SIR substrate is in contact with the line, given by

$$\omega_{p,REF} = \sqrt{\omega_{0,REF}^2 + \frac{1}{LC_p}} \quad (21)$$

as deduced by forcing the denominator of (6) to be null. Another option is to set the frequency of operation to the value where the phase experiences a jump, i.e., $\phi_r = \pm 180^\circ$. Such angular frequency, designated as $\omega_{z,REF}$, is the one that nulls the numerator of (6). It can be analytically deduced, but the resulting expression is complex and hence is not given. Moreover, such jump frequency can be easily identified from the phase response.

The sensitivity analysis for sensor operation at either $\omega_{p,REF}$ or $\omega_{z,REF}$ is by far more complex than for sensor operation at $\omega_{0,REF}$. Therefore, we have not included such analysis in the paper (nevertheless, the sensitivity for sensor operation at such frequencies can be inferred by electromagnetic simulation).

IV. SENSOR VALIDATION

For sensor validation, we have considered the static element and SIR substrate and dimensions used for the parameter extraction and model validation of Section II. The dependence of the phase of the transmission coefficient at $f_{0,REF} = \omega_{0,REF}/2\pi = 2.68$ GHz with the vertical distance, g , as inferred from electromagnetic simulation using the *Ansys High Frequency Structure Simulator (HFSS)* commercial software, is depicted in Fig. 4. In such simulations, we have considered steps in the vertical distance, g , of 2 μm for separations below 10 μm . Then, we have obtained the phases for $g = 50$ μm , 100 μm , 200 μm , 400 μm , 600 μm , 800 μm , and 1000 μm .

Next, we have obtained the same phase dependence experimentally. For that purpose, we have used the *Agilent N5221A* vector network analyzer, and we have obtained the phase of the transmission coefficient for specific vertical distances, g , separated 5 μm when the vertical displacements are below 500 μm , and more distant (i.e., 10 μm) for displacements above 500 μm . Vertical motion of the SIR above the static part has been achieved by means of the *Thorlabs MVS010/M* displacement system available in our laboratory. Fig. 5 depicts a picture of the experimental setup, as well as the fabricated static part and SIR. The experimental datapoints are also depicted in Fig. 4 to ease the comparison with the simulated data. Four independent experiments have been carried out at different instants of time for each vertical distance to guarantee that the device exhibits good repeatability. The experimental curves are almost undistinguishable, and the agreement between the experimental datapoints and the simulations is reasonably good. Indeed, rather than the four experimental responses, in Fig.

4 we have represented the mean value of the four independent measurements corresponding to each vertical displacement, as well as the error bars, given by the standard deviation. However, the standard deviation is very small, and it cannot be appreciated in the scale of the figure. The mean value and error bars after four measurements are also provided for other experimental campaigns, to be discussed later.

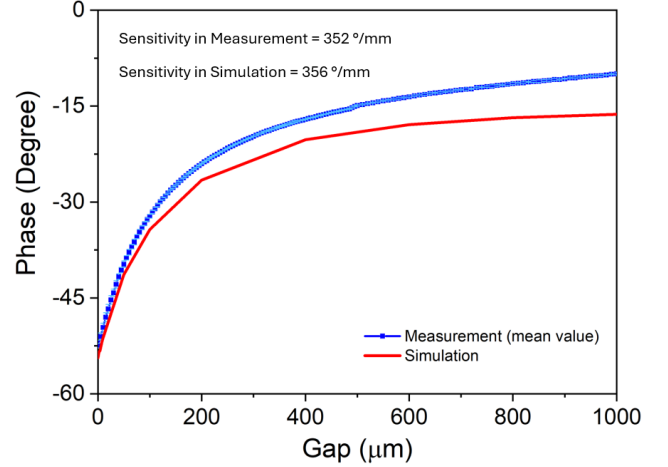


Fig. 4. Dependence of the phase of the transmission coefficient at $f_{0,REF}$ as a function of g for the proposed proximity sensor, designated as sensor A, inferred from electromagnetic simulation and experimentally. The sensitivity in the limit when $g = 0$ μm , as inferred from the derivative of the simulated and measured datapoints, is included.

Concerning the sensitivity in the limit of small vertical displacements, the values that result from the experimental data, the simulations, and the prediction of the theory [expression (20)] are $S_{Exp} = 352^\circ/\text{mm}$, $S_{Sim} = 356^\circ/\text{mm}$, and $S_{Th} = 590^\circ/\text{mm}$, respectively. The reason for the overestimation of the theoretical sensitivity is the fact that the parallel plate capacitor formula provides a capacitance value, C , below the one extracted from the method reported before. Moreover, there is another source of discrepancy, i.e., the parasitic capacitance between the SIR patches and the ground plane, which has been ignored in the model. This assumption is acceptable according to the reasonable agreement between the circuit and electromagnetic simulations in Fig. 3, and necessary to avoid an excessively complex sensitivity analysis, but prevents from obtaining a more accurate prediction of the sensitivity. Thus, considering the above approximations, expression (20) provides an estimation, rather than an accurate prediction of the sensitivity in the limit of small perturbations. Sensor resolution is 5 μm , a competitive value that points out that the proposed sensor is useful for detecting small displacements, or proximity, at the micrometer scale.

We have also obtained the phase response of the sensor for operation at $f_{p,REF} = \omega_{p,REF}/2\pi = 2.96$ GHz and $f_{z,REF} = \omega_{z,REF}/2\pi = 3.51$ GHz. The results are depicted in Fig. 6. The sensitivities in the limit when $g \rightarrow 0$ μm inferred from simulation and measurement are $S_{Sim} = 602^\circ/\text{mm}$ and $S_{Exp} = 626^\circ/\text{mm}$, respectively, for operation at $f_{p,REF}$, and $S_{Sim} = 157^\circ/\text{mm}$ and $S_{Exp} = 255^\circ/\text{mm}$, respectively, for operation at $f_{z,REF}$. Nevertheless, the overall agreement for operation at these frequencies, according to Fig. 6, is good.

Besides sensor A, we have fabricated two additional sensors, in order to obtain improved sensitivities. The device designated as sensor B is identical to sensor A, the unique difference being the thickness of the SIR substrate ($h_{\text{SIR}} = 0.2 \text{ mm}$). Figure 7 depicts the phase dependence with g , for operation at the three considered frequencies, indicated in Table II, where the main relevant characteristics of the sensors are summarized. Note that, as compared to sensor A, sensor B is expected to exhibit an SIR capacitance (in the limit when $g \rightarrow 0 \text{ }\mu\text{m}$) approximately 4 times higher (according to the parallel plate capacitor formula such capacitance is inversely proportional to the SIR substrate thickness). Therefore, the resonance frequency should be roughly 2 times smaller [see expression (1)], and the sensitivity for sensor operation at that frequency should be 2 times higher [see expression (20)], as corroborated from the values depicted in the table, i.e., $S_{\text{Sim}} = 679^\circ/\text{mm}$ and $S_{\text{Th}} = 1014^\circ/\text{mm}$ for operation at $f_{0,\text{REF}}$. The sensitivity of sensor B, inferred from the measured datapoints is $S_{\text{Exp}} = 498^\circ/\text{mm}$, $S_{\text{Exp}} = 663^\circ/\text{mm}$, and $S_{\text{Exp}} = 125^\circ/\text{mm}$, for operation at $f_{0,\text{REF}}$, $f_{p,\text{REF}}$, and $f_{z,\text{REF}}$, respectively, in relative good agreement with the sensitivities inferred from the simulated datapoints (see Table II).

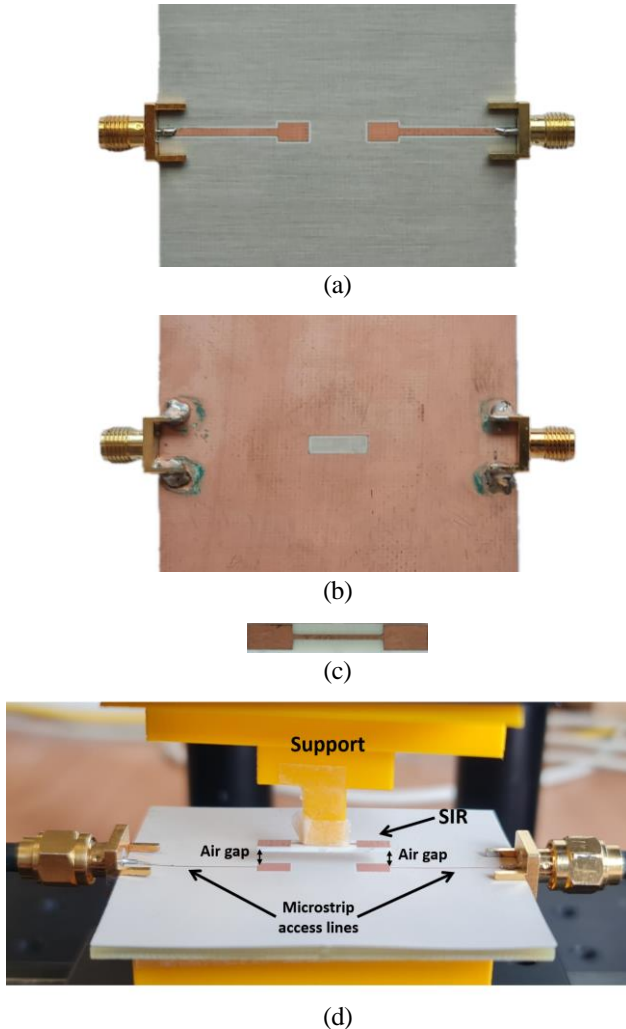


Fig. 5. Photograph of the (a) front side of the static part, (b) back side of the static part, (c) movable part, and (d) experimental setup.

TABLE II
SENSITIVITIES AND OPERATING FREQUENCIES FOR DIFFERENT PROXIMITY SENSORS AS INFERRED FROM SIMULATION

SENSOR	h_{SIR} (μm)	h_{MS} (μm)	ϵ_r	$f_{0,\text{REF}}$ $S_{\text{Sim}}/S_{\text{Th}}$	$f_{p,\text{REF}}$ S_{Sim}	$f_{z,\text{REF}}$ S_{Sim}
A	810	508	3.55	2.683 GHz 356°/590°/mm	2.961 GHz 602°/mm	3.513 GHz 157°/mm
B	200	508	3.55	1.560 GHz 679°/1014°/mm	2.139 GHz 790°/mm	3.257 GHz 115°/mm
C	810	254	10.2	2.628 GHz 54°/603°/mm	2.741 GHz 106°/mm	2.945 GHz 5637°/mm

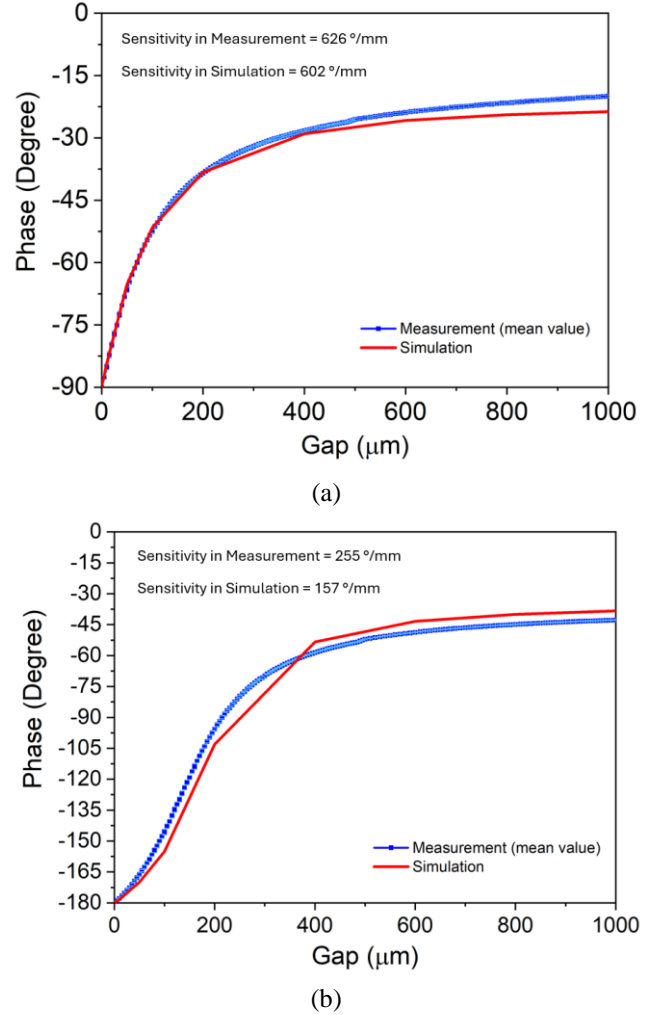


Fig. 6. Dependence of the phase of the transmission coefficient at $f_{p,\text{REF}}$ (a) and at $f_{z,\text{REF}}$ (b) as a function of g for the proximity sensor A inferred from electromagnetic simulation and experimentally. The indicated sensitivities in simulation and measurement correspond to $g = 0 \text{ }\mu\text{m}$.

The sensitivities for sensors A and B in the limit of small separations ($g \rightarrow 0 \text{ }\mu\text{m}$) and operation at $f_{0,\text{REF}}$ and $f_{p,\text{REF}}$ are good, but smaller than the sensitivity reported in [75]. It has been found that by increasing the capacitance C_p , the phase slope at the frequency where the phase of the transmission coefficient is $\phi_T = \pm 180^\circ$ dramatically increases. To boost up C_p by maintaining unaltered the area of the microstrip and SIR patches, increasing the dielectric constant of the static element substrate and/or reducing its thickness are possible solutions. Thus, we have carried out electromagnetic simulations of a new sensor (sensor

C), identical to sensor A, except for the static element substrate, which is now the *Rogers RO3010* with dielectric constant $\epsilon_r = 10.2$, thickness $h_{MS} = 0.254$ mm, and loss tangent $\tan\delta = 0.0022$. The dependence of the phase of the transmission coefficient with g , for the three considered frequencies, is depicted in Fig. 8. The figure includes also the measured data (the photograph is not provided since the geometry is identical of that of Sensor A). The resulting sensitivities (for $g \rightarrow 0$ μm) are $S_{\text{Sim}} = 54^\circ/\text{mm}$ and $S_{\text{Exp}} = 71^\circ/\text{mm}$ for operation at $f_{0,\text{REF}}$, $S_{\text{Sim}} = 106^\circ/\text{mm}$ and $S_{\text{Exp}} = 72^\circ/\text{mm}$ for operation at $f_{p,\text{REF}}$, and $S_{\text{Sim}} = 5637^\circ/\text{mm}$ and $S_{\text{Exp}} = 4485^\circ/\text{mm}$ for operation at $f_{z,\text{REF}}$.

Note that, for sensor C and operation at $f_{0,\text{REF}}$, the sensitivity inferred from the simulated and experimental datapoints is significantly below the prediction by theory, as indicated in Table II ($S_{\text{Th}} = 603^\circ/\text{mm}$). This high discrepancy is attributed to the fact that by reducing the thickness of the static element substrate and by increasing its dielectric constant, the parasitic capacitance between the metal patches of the SIR and the ground plane, not considered in the model (as indicated before), can be significant. Nevertheless, the most relevant aspect of this new sensor C is the high sensitivity achieved at $f_{z,\text{REF}}$ (consequence of the high phase slope at that frequency), pointing out the potential of the proposed structure for the implementation of ultra-highly sensitive proximity sensors.

Let us emphasize that for sensors A and B the effects of the parasitic capacitance are expected to be less severe, as compared to sensor C. Hence, the source of discrepancy between the predictions of the theory and the simulated (or measured) sensitivity in the limit of small displacements for sensors A and B operating at $f_{0,\text{REF}}$ can be mainly attributed to inaccuracies related to the adoption of the parallel plate capacitor formula [see expression (17), that leads to expression (19), and, finally, to expression (20), the one that provides the theoretical sensitivity in the limit of small displacements, S_{Th}]. Thus, we have inferred the sensitivity in the limit of small displacements for sensors A and B by means of an alternative procedure. Particularly, we have calculated the derivative (19) from the extracted capacitances $C(g = 0 \text{ } \mu\text{m}) = C_{\text{REF}}$ (corresponding to the REF position) and $C(g = 10 \text{ } \mu\text{m})$, and by dividing the difference by the increment in the separation g , i.e., 10 μm . The result is then multiplied by (16), providing the sensitivity in the limit of small displacements, according to expression (10). Using such an approach, the prediction is improved. Specifically, for sensor A, we have obtained a sensitivity of $S_{\text{Th}} = 274^\circ/\text{mm}$, closer to the sensitivity inferred from simulation, $S_{\text{Sim}} = 356^\circ/\text{mm}$, and from experiment, $S_{\text{Exp}} = 352^\circ/\text{mm}$. For sensor B, the theoretical sensitivity in the limit of small displacements, as inferred from the described approach, is $S_{\text{Th}} = 465^\circ/\text{mm}$, whereas the simulated and experimental sensitivities in that limit are $S_{\text{Sim}} = 679^\circ/\text{mm}$, and $S_{\text{Exp}} = 498^\circ/\text{mm}$, respectively. These predictions for sensors A and B operating at $f_{0,\text{REF}}$ are better than those that appear in Table II (as S_{Th}). Nevertheless, the accurate prediction of the sensitivity is very difficult since the considered circuit model provides a reasonable (but not a precise) description of the sensor (including the above cited parasitic capacitance, losses, etc., in the circuit model precludes from

carrying out a treatable sensitivity analysis like the one reported in Section III).

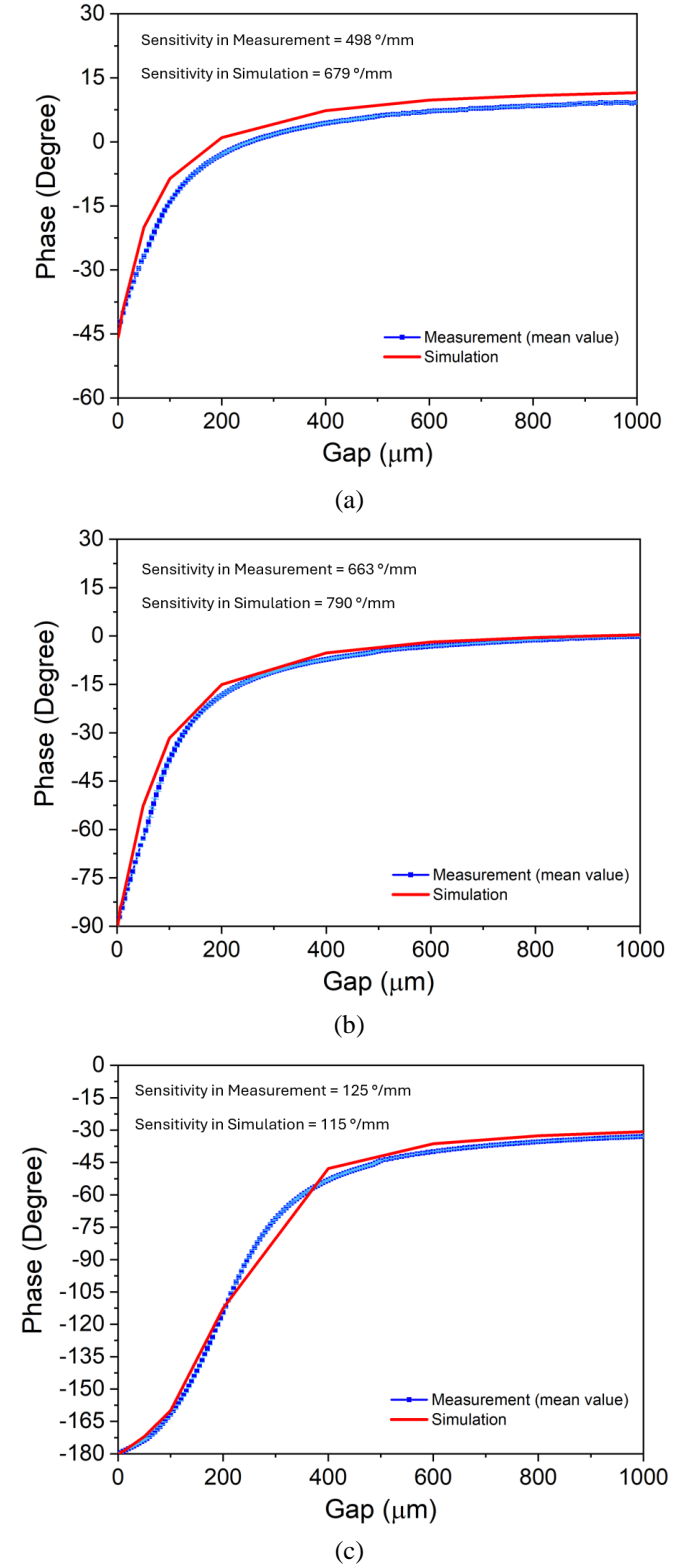


Fig. 7. Dependence of the phase of the transmission coefficient at $f_{0,\text{REF}}$ (a), at $f_{p,\text{REF}}$ (b), and at $f_{z,\text{REF}}$ (c) as a function of g for the proximity sensor B inferred from electromagnetic simulation and experimentally. The indicated sensitivities in simulation and measurement correspond to $g = 0 \text{ } \mu\text{m}$.

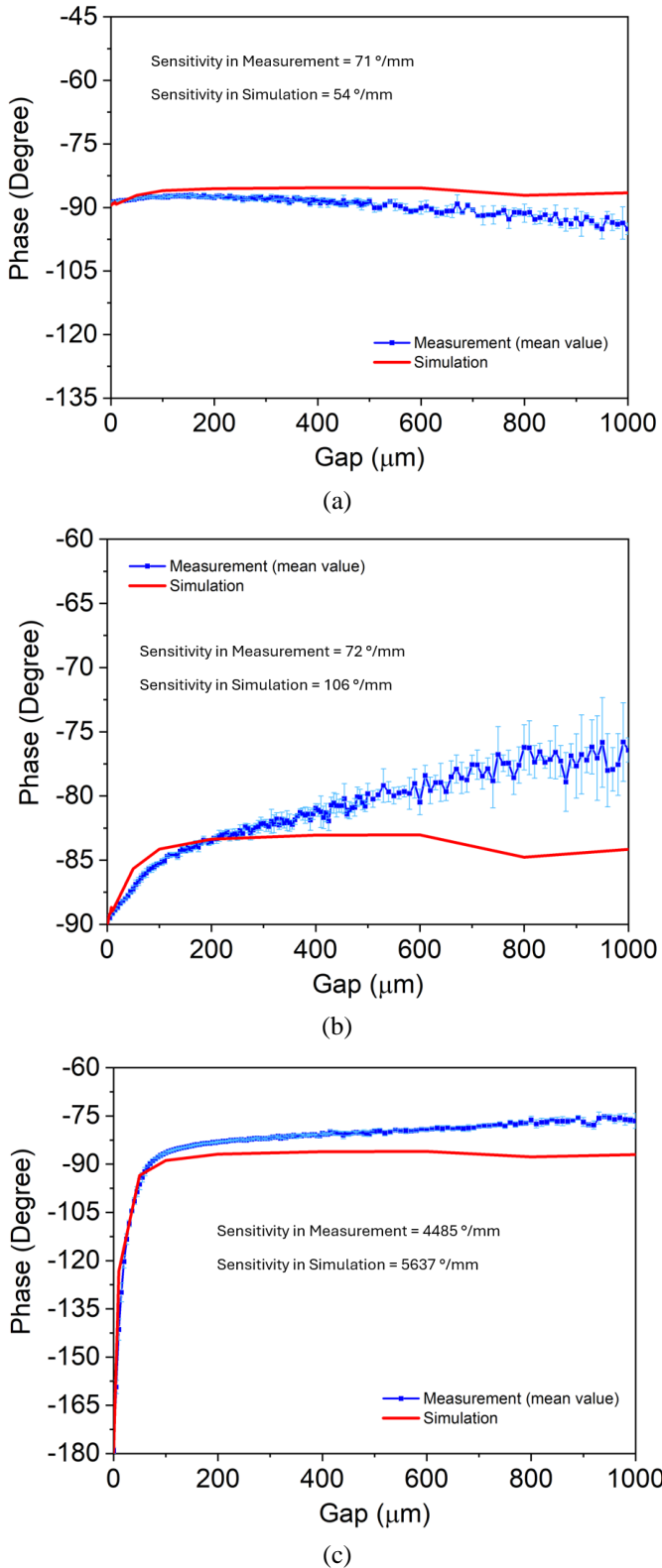


Fig. 8. Dependence of the phase of the transmission coefficient at $f_{0,\text{REF}}$ (a), at $f_{p,\text{REF}}$ (b), and at $f_{z,\text{REF}}$ (c) as a function of g for the proximity sensor C inferred from electromagnetic simulation and experimentally. The indicated sensitivities in simulation and measurement correspond to $g = 0 \mu\text{m}$.

A common feature of the previous sensors, regardless of their specific operating frequency, is the fact that sensitivity

optimization in the limit of small air gaps between the static part and the movable element, the main target in this paper, is achieved at the expense of linearity degradation. Thus, the proposed sensors are of special interest in applications requiring the measurement of proximity in the micrometer scale. Note that the achieved resolution is 5 μm , the limit dictated by our vertical displacement system. Nevertheless, taking into account the achieved sensitivity in the limit when $g \rightarrow 0 \mu\text{m}$ for sensor C operating at $f_{z,\text{REF}}$ (4485 $^\circ/\text{mm}$), it is reasonable to consider that distances smaller than 5 μm can be resolved (for example, by considering that the system is able to discriminate phase differences of 5 $^\circ$, the resulting resolution would be roughly 1 μm).

To end this section, let us mention that regression curves to analytically link the phase with the vertical distance can be obtained. By this means, from the measured phase, the vertical distance can be obtained. Nevertheless, this aspect is out of the scope of the paper, mainly devoted to the design of highly sensitive sensors able to discriminate small distances (micrometer scale) with phase measurements, and to provide design guidelines and strategies to achieve such purpose. Note also that from the anti-image (horizontal axis) of the measured phase in the responses shown in Figs. 4, 6, 7 and 8, the vertical distance, g , can be inferred (nevertheless, for sensor C, see Fig. 8, the frequency of operation should be $f_{z,\text{REF}}$, since at $f_{0,\text{REF}}$ and $f_{p,\text{REF}}$ the sensitivities in the limit of small displacements are low and the phase responses do not exhibit good monotonicity).

V. COMPARATIVE ANALYSIS

Table III includes various microwave proximity sensors reported in the literature (among the fabricated sensors in this work, only sensor C, the one exhibiting the highest sensitivity, is included in the table). Table III reports the maximum sensitivity, resolution, and input dynamic range, the most relevant performance indicator parameters. Note that the sensitivity units are not the same in all sensors. The reason is that some of the sensors in the table are based on frequency variation (with the sensitivity given in MHz/mm), other sensors are based on magnitude variation (the sensitivity units being dB/mm), and, finally, other sensors utilize the phase of either the transmission coefficient (as in this work) or the reflection coefficient as the output variable (and hence the sensitivity is given in $^\circ/\text{mm}$).

In view of Table III, it can be concluded that the proposed sensor C is competitive in terms of sensitivity and resolution. Let us clarify that the maximum sensitivity for sensor C operating at $f_{z,\text{REF}}$ (the one reported in the table) coincides with the sensitivity in the limit of small displacements, but this is not necessarily true in all the reported sensing structures and operation frequencies [for example, for sensor B operating at $f_{z,\text{REF}}$, the maximum sensitivity is found to be in the vicinity of 200 μm , see Fig. 7(c)]. Obviously, the dynamic range is not as good as that of other sensors, because sensitivity and dynamic range are performance indicators that follow opposite trends (optimizing one of them is at the expense of degrading the

other). Nevertheless, we should clarify that the dynamic range is different for the sensors A, B and C reported in this paper, and it depends also on the frequency of operation (the indicators depicted in Table III for sensor C correspond to the frequency of operation that maximizes the sensitivity, i.e., $f_{z,REF}$).

TABLE III
COMPARISON OF VARIOUS MICROWAVE LINEAR
DISPLACEMENT/PROXIMITY SENSORS

Ref.	Maximum sensitivity	Resolution (mm)	Dynamic range (mm)
[18]	110 MHz/mm	0.03	4.0
[21]	80 MHz/mm	< 1	3.0
[22]	95 dB/mm	< 0.05	0.6
[23]	83 dB/mm	< 0.05	0.6
[25]	25 dB/mm	< 0.2	1.0
[26]	26 dB/mm	< 0.1	0.7
[29]	313°/mm	0.016	5.0
[32]	8.0°/mm	0.61	44
[71]	70°/mm	0.5	6.0
[74]	2291°/mm	0.05	< 1.0
[33]	52 MHz/mm	0.5	7.0
[75]	3722°/mm	0.01	< 1.0
[77]	2684°/mm	0.01	< 0.1
Sensor C	4485°/mm	0.005	0.1

Note that the sensitivity and resolution are comparable to those exhibited by the sensor presented in [75], based also on a vertically movable SIR, but operating in reflection and based on a CPW configuration. Both sensors exhibit very high sensitivity because their working principle for measuring proximity is based on the changes generated in a broadside capacitance by vertical motion. Such motion-related capacitance changes are more significant than those that result by vertically moving a dielectric slab on top of a sensing resonator, the strategy used in [71], [74], [77]. Nevertheless, the sensitivities achieved by moving a dielectric slab in the sensors reported in [74], [77] are remarkable. In [74], such high sensitivity (2291°/mm) was achieved by introducing losses in the device (a method that significantly boosts the sensitivity in reflective-mode phase-variation sensors [73], [74], [78]). In [77], the strategy to boost up the sensitivity was to cascade three impedance inverters to the sensing resonator (an open-ended quarter-wavelength resonator). Such sensitivity optimization strategy has also revealed to be very effective [66], but at the expense of adding microwave circuitry to the sensing element (i.e., the inverters). By contrast, the sensors of this work are very simple, as far as they merely consist of the movable SIR and the pair of microstrip patches (the sensor in [74] is also very simple, but it includes a resistive element, either a surface mount device *–smd–* resistor or a junction field effect transistor *–JFET–* operating as a variable conductance).

One advantage of the sensors reported in this work over the sensor in [75] is backside isolation, achieved by implementing such sensors in microstrip technology. Note that the window etched in the ground plane (which prevents from perfect backside isolation) has been etched in order to preserve the value of the inductance L as the SIR moves vertically, since this reduces the complexity of the sensitivity analysis for sensor operation at $f_{0,REF}$. Nevertheless, such a window can be ignored

if good isolation is needed (although in such case the analysis of Section III is not valid).

By operating in transmission, the necessary electronics for sensor operation in real environment (where vector network analyzers should be avoided) is simpler (note that the feeding harmonic signal and the signal containing the relevant information are present at different ports in a transmission-mode sensor). Such readout electronics consist essentially in a phase detector, a microcontroller, and a voltage-controlled oscillator (VCO), the latter necessary to generate the harmonic signal required by the sensing element, i.e., the two-port structure depicted in Fig. 5.

Other capacitive proximity sensors have been proposed [4]–[7], but such sensors are not based on microwave technology for retrieving the input variable (such capacitive sensors are mainly based on impedance measurements). Eddy-current displacement sensors [2], [3] are also competitive, but such sensors can only be applied to conductive moving targets. Other technologies for measuring proximity include Fiber Bragg gratings (FBGs) [79]–[82] and microelectromechanical systems (MEMS) [83]–[86]. In general, the performance of FBG- and MEMS-based proximity sensors, as well as the one of the capacitive proximity sensors based on impedance measurements, is good, but such sensors are relatively complex, as compared to the sensors proposed in this work (simple and cost-effective). Other motion sensors based on kirigami structures have also been proposed [87]–[91]. Applications of the proposed sensors in scenarios requiring proximity/displacement measurements at the micrometer scale can be envisaged (e.g., robotics, ultra-precision machining, automotive and aerospace industry, civil engineering, vibration detection, etc.).

VI. CONCLUSIONS

In conclusion, a new strategy for the implementation of proximity sensors using microwave technology has been proposed. These sensors are two-port transmission-mode devices implemented in microstrip technology that use the phase of the transmission coefficient at a specific (operating) frequency as output variable. The proposed devices are capacitive sensors, as far as the transduction mechanism is the change in the capacitance of a step impedance resonator (SIR), caused by vertical displacement of it with respect to the static part, a pair of lines terminated with metal patches and sharing the same axis. Nevertheless, proximity is measured through microwaves, from the phase of the transmission coefficient at the operating frequency, highly sensitive to vertical displacements. The circuit model of the sensor has been proposed and validated by comparing the electromagnetic responses for different vertical displacements with the circuit responses, inferred from the extracted parameters (a parameter extraction method has also been proposed). From such circuit model, we have reported a sensitivity analysis able to estimate the sensitivity (in the limit of small displacements of the moving target) for sensor operation at the resonance frequency of the SIR. Nevertheless, it has been shown that it is possible to

optimize the sensitivity by tuning the frequency of operation to different frequencies. In particular, it has been found that by considering a narrow and high-dielectric constant microstrip substrate and setting the frequency of operation to the frequency where the phase of the transmission coefficient is $\pm 180^\circ$, the sensitivity can be dramatically boosted up. To demonstrate this, we have designed and experimentally validated a prototype device proximity sensor (designated as sensor C) exhibiting a maximum sensitivity (in the limit of small displacements) as high as $4485^\circ/\text{mm}$ (a result inferred from the measured data). This sensor exhibits a resolution as good as $5\text{ }\mu\text{m}$, which indicates that the sensor is useful for applications requiring micron-level displacement measurements (e.g., ultra-precision machining, robotics, automotive and aerospace industry, etc.).

REFERENCES

- [1] L. Huang, S. Wang, K. Zhang, Y. Li, H. Sui, X. Bu, Y. Jiang, X. Huang, and P. Zhang, "Research progress of multifunctional flexible proximity sensors," *Sens. & Act. A: Phys.*, vol. 360, paper 114500, 2023.
- [2] K. Koibuchi, K. Sawa, T. Honma, T. Hayashi, K. Ueda and H. Sasaki, "Loss estimation and sensing property enhancement for eddy-current-type proximity sensor," *IEEE Trans. Magnetics*, vol. 42, no. 4, pp. 1447-1450, Apr. 2006.
- [3] A. S. Anil Kumar, B. George and S. C. Mukhopadhyay, "An Eddy Current Based Non-Contact Displacement Sensor," *2020 IEEE International Instrumentation and Measurement Technology Conference (I2MTC)*, Dubrovnik, Croatia, 2020, pp. 1-6.
- [4] Y. Ye, C. Zhang, C. He, X. Wang, J. Huang and J. Deng, "A Review on Applications of Capacitive Displacement Sensing for Capacitive Proximity Sensor," *IEEE Access*, vol. 8, pp. 45325-45342, 2020.
- [5] X. Liu, K. Peng, Z. Chen, H. Pu and Z. Yu, "A New Capacitive Displacement Sensor with Nanometer Accuracy and Long Range," *IEEE Sensors J.*, vol. 16, no. 8, pp. 2306-2316, Apr. 2016.
- [6] A. S. Anil Kumar, N. Anandan, B. George and S. C. Mukhopadhyay, "Improved Capacitive Sensor for Combined Angular and Linear Displacement Sensing," *IEEE Sensors J.*, vol. 19, no. 22, pp. 10253-10261, Nov. 2019.
- [7] T. Zeng *et al.*, "A Capacitive Sensor for the Measurement of Departure from the Vertical Movement," *IEEE Trans. Instrum. Meas.*, vol. 65, no. 2, pp. 458-466, Feb. 2016.
- [8] P. Ripka, M. Janosek, "Advances in magnetic field sensors," *IEEE Sensors J.*, vol. 10, pp. 1108-1116, 2010.
- [9] J. Man, G. Chen, J. Chen, "Recent progress of biomimetic tactile sensing technology based on magnetic sensors," *Biosensors*, vol. 12, paper 1054, 2022. <https://doi.org/10.3390/bios12111054>.
- [10] S.D. Min, J.K. Kim, H.S. Shin, Y.H. Yun, C.K. Lee, M. Lee, "Noncontact respiration rate measurement system using an ultrasonic proximity sensor," *IEEE Sensors J.*, vol. 10, pp. 1732-1739, 2010.
- [11] A. Sun, Z. Wu, D. Fang, J. Zhang, W. Wang, "Multimode interference-based fiber optic ultrasonic sensor for non-contact displacement measurement," *IEEE Sensors J.*, vol. 16, pp. 5632-5635, 2016.
- [12] S. Kim, H. Kim, "Optimally overlapped ultrasonic sensor ring design for minimal positional uncertainty in obstacle detection," *Int. J. Control Autom.*, vol. 8, pp. 1280-1287, 2010.
- [13] B.K. Kim, K. Joo, "A multi-channel fiber optic proximity sensor," *Meas. Sci. Technol.*, vol. 27, paper 035104, 2016.
- [14] Y.S. Suh, "Laser sensors for displacement, distance and position," *Sensors*, vol. 19, paper 1924, 2019.
- [15] X. Lin, Y. Liang, L. Jin, L. Wang, "Dual-polarized fiber laser sensor for photoacoustic microscopy," *Sensors*, vol. 19, paper 4632, 2019.
- [16] D. Um, D. Ryu, M. Kal, "Multiple intensity differentiation for 3-D surface reconstruction with mono-vision infrared proximity array sensor," *IEEE Sensors J.*, vol. 11, paper 3352-3358, 2011.
- [17] K. Kito, S. Kitajima, T. Matsuda, M. Inoue, M. Tamura, M. Kimura, "Infrared sensors using poly-Si thin-film transistors for proximity sensors integrated in smartphone displays," *J. Soc. Inf. Disp.*, vol. 27, pp. 147-154, 2019.
- [18] C. Mandel, B. Kubina, M. Schüßler, and R. Jakoby, "Passive chipless wireless sensor for two-dimensional displacement measurement," *41st Europ. Microw. Conf.*, Manchester, UK, Oct. 2011, pp. 79-82.
- [19] A. Ebrahimi, W. Withayachumnankul, S. F. Al-Sarawi, and D. Abbott, "Metamaterial-inspired rotation sensor with wide dynamic range," *IEEE Sensors J.*, vol. 14, no. 8, pp. 2609-2614, Aug. 2014.
- [20] A. K. Jha, A. Lamecki, M. Mrozowski and M. Bozzi, "A Microwave Sensor with Operating Band Selection to Detect Rotation and Proximity in the Rapid Prototyping Industry," *IEEE Trans. Ind. Electron.* vol. 68, no. 1, pp. 683-693, Jan. 2021.
- [21] A. K. Horestani, J. Naqui, Z. Shaterian, D. Abbott, C. Fumeaux, and F. Martín, "Two-dimensional alignment and displacement sensor based on movable broadside-coupled split ring resonators," *Sens. Act. A.*, vol. 210, pp. 18-24, Apr. 2014.
- [22] J. Naqui, M. Durán-Sindreu, and F. Martín, "Novel sensors based on the symmetry properties of split ring resonators (SRRs)," *Sensors*, vol. 11, pp. 7545-7553, 2011.
- [23] J. Naqui, M. Durán-Sindreu, and F. Martín, "Alignment and position sensors based on split ring resonators," *Sensors*, vol. 12, pp. 11790-11797, 2012.
- [24] J. Naqui and F. Martín, "Transmission lines loaded with bisymmetric resonators and their application to angular displacement and velocity sensors," *IEEE Trans. Microw. Theory Techn.*, vol. 61, no. 12, pp. 4700-4713, Dec. 2013.
- [25] A. Karami-Horestani, C. Fumeaux, S. F. Al-Sarawi, and D. Abbott, "Displacement sensor based on diamond-shaped tapered split ring resonator," *IEEE Sensors J.*, vol. 13, no. 4, pp. 1153-1160, Apr. 2013.
- [26] A. K. Horestani, J. Naqui, D. Abbott, C. Fumeaux, and F. Martín, "Two-dimensional displacement and alignment sensor based on reflection coefficients of open microstrip lines loaded with split ring resonators," *Electron Lett.*, vol. 50, no. 8, pp. 620-622, Apr. 2014.
- [27] A. K. Horestani, Z. Shaterian, and F. Martín, "Rotation sensor based on the cross-polarized excitation of split ring resonators (SRRs)," *IEEE Sensors J.*, vol. 20, pp. 9706-9714, Sep. 2020.
- [28] A. K. Jha, A. Lamecki, M. Mrozowski, and M. Bozzi, "A highly sensitive planar microwave sensor for detecting direction and angle of rotation," *IEEE Trans. Microw. Theory Techn.*, vol. 68, no. 4, pp. 1598-1609, Apr. 2020.
- [29] J. Muñoz-Enano, P. Vélez, L. Su, M. Gil, and F. Martín, "A reflective-mode phase-variation displacement sensor", *IEEE Access*, vol. 8, pp. 189565-189575, Oct. 2020.
- [30] Z. Mehrjoo, A. Ebrahimi, G. Beziuk, F. Martín and K. Ghorbani, "Microwave Rotation Sensor Based on Reflection Phase in Transmission Lines Terminated with Lumped Resonators," *IEEE Sensors J.*, vol. 23, no. 7, pp. 6571-6580, Apr. 2023.
- [31] Z. Mehrjoo, A. Ebrahimi, G. Beziuk and K. Ghorbani, "Wideband Amplitude Variation Displacement Sensor in Transmission Mode," *IEEE Sensors J.*, vol. 24, no. 13, pp. 20539-20548, Jul. 2024.
- [32] A. Karami-Horestani, F. Paredes and F. Martín, "Phase-Variation Microwave Displacement Sensor with Good Linearity and Application to Breath Rate Monitoring", *IEEE Sensors J.*, vol. 23, no. 19, pp. 22486-22495, Oct. 2023.
- [33] Z. Mehrjoo, A. Ebrahimi and K. Ghorbani, "Microwave Resonance-Based Reflective Mode Displacement Sensor with Wide Dynamic Range," *IEEE Trans. Instrum. Meas.*, vol. 71, pp. 1-9, Art no. 8000609, 2022.
- [34] F. Martín, C. Herrojo, J. Mata-Contreras, F. Paredes, *Time-Domain Signature Barcodes for Chipless-RFID and Sensing Applications*, Springer, Feb. 2020.
- [35] J. Mata-Contreras, C. Herrojo, and F. Martín, "Application of split ring resonator (SRR) loaded transmission lines to the design of angular displacement and velocity sensors for space applications", *IEEE Trans. Microw. Theory Techn.*, vol. 65, no. 11, pp. 4450-4460, Nov. 2017.
- [36] J. Mata-Contreras, C. Herrojo, and F. Martín, "Detecting the rotation direction in contactless angular velocity sensors implemented with rotors loaded with multiple chains of split ring resonators (SRRs)", *IEEE Sensors J.*, vol. 18, no. 17, pp. 7055-7065, Sep. 2018.
- [37] C. Herrojo, J. Mata-Contreras, F. Paredes, F. Martín, "Microwave encoders for chipless RFID and angular velocity sensors based on S-shaped split ring resonators (S-SRRs)", *IEEE Sensors J.*, vol. 17, pp. 4805-4813, Aug. 2017.
- [38] C. Herrojo, F. Muela, J. Mata-Contreras, F. Paredes, F. Martín, "High-density microwave encoders for motion control and near-field chipless-RFID", *IEEE Sensors J.*, vol. 19, pp. 3673-3682, May 2019.
- [39] C. Herrojo, F. Paredes, and F. Martín, "Double-stub loaded microstrip line reader for very high data density microwave encoders", *IEEE Trans. Microw. Theory Techn.*, vol. 67, no. 9, pp. 3527-3536, Sep. 2019.

- [40] C. Herrojo, F. Paredes, and F. Martín, "3D-printed high data-density electromagnetic encoders based on permittivity contrast for motion control and chipless-RFID", *IEEE Trans. Microw. Theory Techn.*, vol. 68, no. 5, pp. 1839-1850, May 2020.
- [41] F. Paredes, C. Herrojo, F. Martín, "Microwave Encoders with Synchronous Reading and Direction Detection for Motion Control Applications", *2020 IEEE-MTT-S Int. Microw. Symp. (IMS'20)*, Los Angeles, CA, USA, 21-26 Jun. 2020.
- [42] C. Herrojo, F. Paredes, and F. Martín "Synchronism and Direction Detection in High-Resolution/High-Density Electromagnetic Encoders", *IEEE Sensors J.*, vol. 21, no. 3, pp. 2873-2882, Feb. 2021.
- [43] F. Paredes, C. Herrojo, F. Martín, "3D-printed quasi-absolute electromagnetic encoders for chipless-RFID and motion control applications", *Electronics*, vol. 10, paper 1154, May. 2021.
- [44] F. Paredes, C. Herrojo, A. Moya, M. Berenguel-Alonso, D. Gonzalez, J. Bruguera, C. Delgado-Simao, and F. Martín, "Electromagnetic Encoders Screen-Printed on Rubber Belts for Absolute Measurement of Position and Velocity", *Sensors*, vol. 22, paper 2044, Mar. 2022.
- [45] A. Karami-Horestani, F. Paredes and F. Martín, "Frequency-coded and programmable synchronous electromagnetic encoders based on linear strips", *IEEE Sensors Lett.*, vol. 6, no. 8, pp. 1-4, Art no. 3501704, Aug. 2022.
- [46] A. Karami-Horestani, F. Paredes and F. Martín, "High data density absolute electromagnetic encoders based on hybrid time/frequency domain encoding", *IEEE Sensors J.*, vol. 22, no. 24, pp. 23866-23876, Oct. 2022.
- [47] F. Paredes, A. Moya, M. Berenguel-Alonso, D. Gonzalez, J. Bruguera, C. Delgado-Simao, and F. Martín, "Motion Control System for Industrial Scenarios Based on Electromagnetic Encoders", *IEEE Trans. Instrum. Meas.*, vol. 72, pp. 1-12, Art no. 2003612, 2023.
- [48] A. Karami-Horestani, F. Paredes, and F. Martín, "Synchronous Electromagnetic Encoders Based on Step-Impedance Resonators", *IEEE Sensors J.*, vol. 23, no. 19, pp. 22440-22450, Oct. 2023.
- [49] A. Karami-Horestani, F. Paredes and F. Martín, "Hybrid Time/Phase Domain Synchronous Electromagnetic Encoders for Near-Field Chipless-RFID and Motion Control Applications," *IEEE Trans. Microw. Theory Techn.*, vol. 71, no. 12, pp. 5457-5469, Dec. 2023.
- [50] E. Eitel, "Basics of Rotary Encoders: Overview and New Technologies," *Machine Design Mag.*, vol. 4, no. 2, May. 2014.
- [51] G. K. McMillan and D. M. Considine, "Process/Industrial Instrument and Control Handbook," in *Symp. A Quarterly J. In Modern Foreign Literatures*, 1999.
- [52] X. Li, J. Qi, Q. Zhang, and Y. Zhang, "Bias-tunable dual-mode ultraviolet photodetectors for photoelectric tachometer," *Appl. Phys. Lett.*, vol. 104, no. 4, paper 041108, Jan. 2014.
- [53] Z. Zhang, Y. Dong, F. Ni, M. Jin, and H. Liu, "A Method for Measurement of Absolute Angular Position and Application in a Novel Electromagnetic Encoder System," *J. Sensors*, vol. Apr. 2015, doi: 10.1155/2015/503852.
- [54] Z. Zhang, F. Ni, Y. Dong, M. Jin, and H. Liu, "A novel absolute angular position sensor based on electromagnetism," *Sens. & Act., A: Phys.*, vol. 194, May. 2013, doi: 10.1016/j.sna.2013.01.040.
- [55] J. Jezný, and M. Curilla, "Position Measurement with Hall Effect Sensors", *Am. J. Mech. Eng.*, vol. 1, pp. 231-235, Jan. 2013.
- [56] P.N. Granell, G. Wang, G. S. Cañon Bermudez, T. Kosub, F. Golmar, L. Steren, J. Fassbender, and D. Makarov, "Highly compliant planar Hall effect sensor with sub 200 nT sensitivity," *Npj Flex. Electron.*, vol. 3, p. 3, Feb. 2019.
- [57] A. Lidozzi, L. Solero, F. Crescimbeni, and A. Di Napoli, "SVM PMSM Drive with Low Resolution Hall-Effect Sensors," *IEEE Trans. Power Electr.*, vol. 22, pp. 282-290, Jan. 2007.
- [58] G. Scelba, G. De Donato, G. Scarella, F. Giulii Capponi, and F. Bonaccorso, "Fault-Tolerant Rotor Position and Velocity Estimation Using Binary Hall-Effect Sensors for Low-Cost Vector Control Drives," *IEEE Trans. Ind. Appl.*, vol. 50, pp. 3403-3413, Feb. 2014.
- [59] X. Zhang, M. Mehrtash, M.B. Khamesee, "Dual-Axial Motion Control of a Magnetic Levitation System Using Hall-Effect Sensors," *IEEE/ASME Trans. Mechatron.*, vol. 21, pp. 1129-1139, Sep. 2015.
- [60] G. Liu, B. Chen, and X. Song, "High-Precision Speed and Position Estimation Based on Hall Vector Frequency Tracking for PMSM with Bipolar Hall-Effect Sensors," *IEEE Sensors J.*, vol. 19, pp. 2347-2355, Dec. 2018.
- [61] F. Martín, P. Vélez, J. Muñoz-Enano, L. Su, *Planar Microwave Sensors*, Wiley/IEEE Press, Hoboken, NJ, USA, 2022.
- [62] A. V. Praveen Kumar and P. Regalla, "A Transmission Mode Dielectric Resonator as a Displacement Sensor," *IEEE Sensors J.*, vol. 20, no. 13, pp. 6979-6984, Jul. 2020.
- [63] P. Regalla and A. V. P. Kumar, "A Fixed-Frequency Angular Displacement Sensor Based on Dielectric-Loaded Metal Strip Resonator," *IEEE Sensors J.*, vol. 21, no. 3, pp. 2669-2675, Feb. 2021.
- [64] P. Regalla and A. V. P. Kumar, "Two-Dimensional Wide Dynamic Range Displacement Sensor Using Dielectric Resonator Coupled Microwave Circuit," *IEEE Sensors J.*, vol. 23, no. 24, pp. 30222-30230, Dec. 2023.
- [65] P. Regalla and A. V. Praveen Kumar, "A low-cost reflection mode operated microwave resonator sensor for angular displacement detection," *J. Electromagn. Waves Appl.*, vol. 38, no. 15, pp. 1621-1634, 2024.
- [66] J. Muñoz-Enano, P. Vélez, L. Su, M. Gil, P. Casacuberta, and F. Martín, "On the sensitivity of reflective-mode phase variation sensors based on open-ended stepped-impedance transmission lines: theoretical analysis and experimental validation", *IEEE Trans. Microw. Theory Techn.* vol. 69, no. 1, pp. 308-324, Jan. 2021.
- [67] L. Su, J. Muñoz-Enano, P. Vélez, M. Gil, P. Casacuberta, and F. Martín, "Highly sensitive reflective-mode phase-variation permittivity sensor based on a coplanar waveguide (CPW) terminated with an open complementary split ring resonator (OCSRR)," *IEEE Access*, vol. 9, pp. 27928-27944, 2021.
- [68] P. Casacuberta, P. Vélez, J. Muñoz-Enano, L. Su, M. Gil, A. Ebrahimi and F. Martín, "Circuit analysis of a Coplanar waveguide (CPW) terminated with a step-impedance resonator (SIR) for highly sensitive one-port permittivity sensing," *IEEE Access*, vol. 10, pp. 62597-62612, 2022.
- [69] J. Muñoz-Enano, P. Vélez, P. Casacuberta, L. Su, and F. Martín, "Reflective-Mode Phase-Variation Permittivity Sensor Based on a Step-Impedance Microstrip Line Terminated with a Slot Resonator for Solid and Liquid Characterization", *IEEE Trans. Microw. Theory Techn.*, vol. 72, no. 4, pp. 2519-2533, Apr. 2024.
- [70] P. Vélez, X. Canalias, J. Muñoz-Enano, P. Casacuberta, L. Su, and F. Martín, "Effects of Losses on the Sensitivity of Reflective-Mode Phase-Variation Liquid Sensors", *IEEE Trans. Microw. Theory Techn.* vol. 72, no. 2, pp. 903-918, Feb. 2024.
- [71] P. Casacuberta, P. Vélez, J. Muñoz-Enano, L. Su, and F. Martín, "Highly sensitive reflective-mode phase-variation permittivity sensors using coupled line sections", *IEEE Trans. Microw. Theory Techn.*, vol. 71, pp. 2970-2984, Jul. 2023.
- [72] P. Casacuberta, P. Vélez, J. Muñoz-Enano, L. Su, and F. Martín, "Highly Sensitive Coplanar Waveguide (CPW) Reflective-Mode Phase-Variation Permittivity Sensors Based on Weakly Coupled Step-Impedance Resonators (SIRs)," *IEEE Trans. Microw. Theory Techn.*, vol. 72, no. 3, pp. 1739-1753, Mar. 2024.
- [73] P. Casacuberta, P. Vélez, J. Muñoz-Enano, L. Su, and F. Martín, "Losses-assisted sensitivity enhancement in reflective-mode phase-variation permittivity sensors based on weakly coupled distributed resonators", *IEEE Sensors Lett.*, vol. 7, Art no. 1500704, Aug. 2023.
- [74] P. Casacuberta, P. Vélez, L. Su, X. Canalias, Ferran Martín, "Highly sensitive lossy tunable permittivity sensor", *IEEE Microw. Wireless Technol. Lett.*, vol. 34, no. 6, pp. 687-690, Jun. 2024.
- [75] A. Karami-Horestani, F. Paredes, P. Casacuberta, A. Ebrahimi, P. Vélez, K. Adolphs, K. Ghorbani, and F. Martín, "Reflective-mode phase-variation sensors based on a movable step impedance resonator (SIR) and application to micrometer-scale motion sensing", *IEEE Trans. Microw. Theory Techn.*, doi: 10.1109/TMTT.2024.3423407.
- [76] D. M. Pozar, *Microwave Engineering*, 4th Ed., John Wiley, Hoboken, NJ, USA, 2011.
- [77] X. Canalias, P. Vélez, P. Casacuberta, L. Su, and F. Martín "Transmission-Mode Phase-Variation Planar Microwave Sensor Based on a Step-Impedance Shunt Stub for High Sensitivity Defect Detection, Dielectric Constant, and Proximity Measurements", *IEEE Trans. Microw. Theory Techn.*, doi: 10.1109/TMTT.2024.3429536.
- [78] P. Casacuberta, P. Vélez, L. Su, X. Canalias, and F. Martín "Engineering with Loss to Enhance Sensitivity in Microwave Sensors", *IEEE Microw. Mag.*, doi: 10.1109/MMM.2024.3474636.
- [79] T. Li, C. Shi and H. Ren, "A Novel Fiber Bragg Grating Displacement Sensor with a Sub-Micrometer Resolution," *IEEE Photonics Technol. Lett.*, vol. 29, no. 14, pp. 1199-1202, Jul. 2017.
- [80] L. Xiong, Y. Guo, G. Jiang, L. Jiang and X. Zhou, "Fiber Bragg Grating Displacement Sensor with High Measurement Accuracy for Crack Monitoring," *IEEE Sensors J.*, vol. 19, no. 22, pp. 10506-10512, Nov. 2019.
- [81] Y. Guo, W. Zhou, L. Xiong, X. Zhou and L. Li, "A Fiber Bragg Grating Sensor for Positive and Negative Displacement Measurement," *IEEE Sensors J.*, vol. 21, no. 19, pp. 21564-21571, Oct. 2021.
- [82] M. Bonopera, "Fiber-Bragg-Grating-Based Displacement Sensors: Review of Recent Advances," *Materials*, vol. 15, no. 16, p. 5561, 2022.

- [83] H. Sekiya, K. Kimura, and C. Miki, "Technique for Determining Bridge Displacement Response Using MEMS Accelerometers," *Sensors*, vol. 16, no. 2, p. 257, 2016.
- [84] A. M. Kamal, S. H. Hemel and M. U. Ahmad, "Comparison of Linear Displacement Measurements Between a Mems Accelerometer and Hc-Sr04 Low-Cost Ultrasonic Sensor," *2019 1st International Conference on Advances in Science, Engineering and Robotics Technology (ICASERT)*, Dhaka, Bangladesh, 2019, pp. 1-6.
- [85] W-M Niu, F. Li-qing, Z-Y. Qi, and D.Q Guo, "Small Displacement Measuring System Based on MEMS Accelerometer," *Mathematical Problems in Engineering*, Vol. 2019, Article ID 3470604, 7 pages, 2019.
- [86] M. N. Horenstein, J. A. Perreault, and T. G. Bifano, "Differential capacitive position sensor for planar MEMS structures with vertical motion," *Sens. & Act.*, vol 80, pp. 53–61, 2000.
- [87] Y. Hong *et al.*, "Highly anisotropic and flexible piezoceramic kirigami for preventing joint disorders," *Sci. Adv.*, vol. 7, paper eabf0795, 2021.
- [88] M. Hashimoto and Y. Taguchi, "Design and Fabrication of a Kirigami-Inspired Electrothermal MEMS Scanner with Large Displacement," *Micromachines*, vol. 11, no. 4, paper 362, 2020.
- [89] S. Charkhabi *et al.*, "Kirigami-Enabled, Passive Resonant Sensors for Wireless Deformation Monitoring," *Adv. Mater. Technol.*, vol. 4, paper 1800683, 2019.
- [90] A. Salim, O. Niksan and M. H. Zarifi, "Kirigami Integrated Yagi-Uda Antenna for Strain Sensing in Biomedical Applications," *2023 IEEE MTT-S International Microwave Biomedical Conference (IMBioC)*, Leuven, Belgium, 2023, pp. 172-174.
- [91] Z. A. Dijvejin, K. K. Kazemi, K. Alasvand Zarasvand, M. H. Zarifi, and K. Golovin, "Kirigami-Enabled Microwave Resonator Arrays for Wireless, Flexible, Passive Strain Sensing," *ACS Appl. Mater. Interfaces*, vol. 12, no. 39, pp. 44256-44264, 2020.



Amirhossein Karami Horestani has got his bachelor's degree in 2015 in the field of biomedical engineering from the University of Isfahan. Then he studies at the University of Tehran in the field of micro/nano electronics for the master's degree until 2018. Since December 2021 he is working on microwave sensors and near-field RFID systems as a PhD student at Universitat Autònoma de Barcelona.



Ferran Paredes (M'14-SM'22) received the Telecommunications Engineering degree from the Universitat Autònoma de Barcelona in 2006 and the PhD degree in Electronics Engineering from the same university in 2012. He is working as a Associate Professor at the Universitat Autònoma de Barcelona and his research interests include metamaterial concepts, passive microwaves devices, antennas, and RFID.



Karl Adolphs Saura was born in Sabadell, Barcelona, Spain, in 1999. He received the bachelor's degree in telecommunication systems engineering and the master's degree in telecommunications engineering from the Universitat Autònoma de Barcelona (UAB), Spain, in 2022 and 2024, respectively. He is currently focused on microwave encoders based on reflective-mode phase-variation sensors and tags based on permittivity contrast.



Amir Ebrahimi (S'09, M'16) received the B.Sc. degree in electrical engineering in 2008, the M.Sc. degree in microelectronics in 2011, and the Ph.D. degree from the University of Adelaide, Adelaide, Australia in 2016. He is now a Senior Research Fellow in the School of Engineering, RMIT University, Melbourne, Australia. He was a Visiting Research Fellow at Nanyang Technological University (NTU), Singapore, during 2014-2015. His research interests include

metamaterial inspired microwave devices, microwave circuit design, microwave filters, frequency-selective surfaces (FSSs) and nonlinear RF, and microwave circuits design and analysis.

Dr. Ebrahimi was a recipient of the Australian National Fabrication Facility (ANFF) Award (2013), the University of Adelaide D.R. Stranks Traveling Fellowship (2014), the Yarman–Carlin Best Student Paper Award at the Mediterranean Microwave Symposium (2015), the Simon Rockliff Scholarship (2016), the Best Paper award at the Australian Microwave Symposium (2016), Gertrude Rohan Memorial Prize (2017), and the CASS Foundation travel award (2019). Since 2023 he is serving as an Associate Editor of the IEEE Sensors Journal. He is a reviewer for several recognized international journals such as IEEE Transactions on Microwave Theory and Techniques, IEEE Transactions on Antennas and Propagations, and IEEE Microwave and Wireless Components Letters.



Ferran Martín (M'04-SM'08-F'12) was born in Barakaldo (Vizcaya), Spain in 1965. He received the B.S. Degree in Physics from the Universitat Autònoma de Barcelona (UAB) in 1988 and the PhD degree in 1992. From 1994 up to 2006 he was Associate Professor in Electronics at the Departament d'Enginyeria Electrònica (UAB), and since 2007 he is Full Professor of Electronics. Throughout his career, he has been very active in research fields as diverse as metamaterials and

artificial transmission lines, microwave circuits and filters, antennas, chipless-RFID, and planar microwave sensors (his main research topic at present). He is the head (and founder) of the Microwave Engineering, Metamaterials and Antennas Group (GEMMA Group) at UAB, and director (and founder) of CIMITEC, a research and technology transfer Center ascribed to the Departament d'Enginyeria Electrònica (UAB). He has organized several international events related to metamaterials, chipless-RFID, and sensors, including Workshops at the IEEE International Microwave Symposium (years 2005 and 2007) and European Microwave Conference (2009, 2015, 2017, 2018, and 2024), and the Fifth International Congress on Advanced Electromagnetic Materials in Microwaves and Optics (Metamaterials 2011), where he acted as Chair of the Local Organizing Committee. He has acted as Guest Editor for seven Special Issues on metamaterials and sensors in various International Journals. He has authored and co-authored over 700 technical conference, letter, journal papers and book chapters, he is co-author of the book on Metamaterials entitled *Metamaterials with Negative Parameters: Theory, Design and Microwave Applications* (John Wiley & Sons Inc.), author of the book *Artificial Transmission Lines for RF and Microwave Applications* (John Wiley & Sons Inc.), co-editor of the book *Balanced Microwave Filters* (Wiley/IEEE Press), co-author of the book *Time-Domain Signature Barcodes for Chipless-RFID and Sensing Applications* (Springer), co-author of the book *Planar Microwave Sensors* (Wiley/IEEE Press), and co-Editor of the book *Coupled Structures for Microwave Sensing* (Springer). Ferran Martín has generated 22 PhDs, has filed several patents on metamaterials, chipless-RFID, and sensors, and has headed dozens of development contracts and collaborative projects with companies.

Prof. Martín is a member of the IEEE Microwave Theory and Techniques Society (IEEE MTT-S). He is reviewer of the IEEE TRANSACTIONS ON MICROWAVE THEORY AND TECHNIQUES and IEEE MICROWAVE AND WIRELESS COMPONENTS LETTERS, among many other journals, and he serves as member of the Editorial Board of IEEE TRANSACTIONS ON MICROWAVE THEORY AND TECHNIQUES, IET MICROWAVES, ANTENNAS AND PROPAGATION, and Sensors. He is also a member of the Technical Program Committee of the European Microwave Conference (EuMC) and member of the Scientific Advisory Board of the International Congress on Advanced Electromagnetic Materials in Microwaves and Optics (Metamaterials). Among his distinctions, Ferran Martín has received the 2006 Duran Farell Prize for Technological Research, he holds the *Parc de Recerca UAB – Santander Technology Transfer Chair*, and he has been the recipient of three ICREA ACADEMIA Awards (calls 2008, 2013 and 2018). He is Fellow of the IEEE and Fellow of the IET.